Conformational Coupling of the Nucleotide-Binding and the Transmembrane Domains in ABC Transporters

Po-Chao Wen and Emad Tajkhorshid

Center for Biophysics and Computational Biology, Department of Biochemistry, College of Medicine, and Beckman Institute for Advanced Science and Technology, University of Illinois at Urbana-Champaign, Urbana, Illinois

Supplemental Materials

Construction of Simulation Systems

The models used for the MD simulations are based on the crystal structure of the *Escherichia coli* maltose transporter MalEFGK in its nucleotide-bound, substrate-associated state (PDB entry: 2R6G (1)). The unresolved loops of MalF:D243–G244 and MalG:E68–R73 were not modeled, and a peptide bond was used to directly connect the C-terminus of MalG:V67 and the N-terminus of MalG:I74, as if deleting mutations occurred in between. The ATPase-suppressing MalK:E159Q mutation was reversed in both NBDs.

The two ATP molecules of the NBDs in the crystal structure were replaced by MgATP. Because the orientation of the β- and the γ-phosphates in this crystal structure does not support a 6-coordinated Mg^{2+} in the position seen in other MgATP-bound structures of ABC transporters, the MgATP needed to be modeled using other structural references. Two crystal structures of isolated, ATP-bound NBDs were adopted for this purpose: MalK (PDB:1Q12 (2)) and MJ0796 (PDB:1L2T (3)). Specifically, the structures were superimposed on the MgATP-binding part of the Walker A motifs (using the backbone atoms of MalK:S38–T43 and MJ0796:S40–S45), and the MgATP was modeled using the coordinates of ATP from the MalK reference structure, with the Mg^{2+} adopting the coordinate of the Na^{+} from the MJ0796 structure. A 3000-step energy minimization was performed, resulting in a stable model without any major conformational changes in the protein. Of particular importance, the placed Mg^{2+} established coordination with the Q-loop glutamine MalK:Q82 in both active sites already during the minimization period.

The model of the intact transporter was then embedded in a lipid bilayer consisting of 373 POPE molecules (180 and 193 lipids in the periplasmic and the cytoplasmic leaflets, respectively), and solvated in a periodic water box with 100 mM of NaCl, resulting in a simulation system of ∼320,000 atoms, with approximate dimensions of $130 \times 130 \times 200\,\text{Å}^3$ before equilibration.

Equilibrium MD simulations were performed using NAMD 2.6 (4). The CHARMM27 force field (5–7), including the ϕ/ψ cross-term map (CMAP) correction for the proteins (5) was used for all the simulations. Water molecules were described with the TIP3P model (8). The bound substrate of the transporter, maltose, was represented with the CHARMM Car-

bohydrate Solution Force Field (CSFF) (9).

Simulations were carried out at 310 K constant temperature using Langevin dynamics with a damping coefficient γ of 0.5 ps^{-1}. The pressure along the membrane normal (the z-axis of the simulation system) was maintained at 1 atm using the Nosé-Hoover Langevin piston method (10; 11), with a constant cross-sectional area imposed on the xy-plane unless specified otherwise. The cutoff distance for non-bonded interactions was set to 12 Å, and long-range electrostatic interactions were computed with the particle mesh Ewald (PME) method (12).

The equilibration of the system started with the acyl chains of the lipid molecules ("melting") under constant volume conditions for 0.5 ns, with all other atoms assigned to fixed coordinates. The system was then further simulated with all protein atoms restrained ($k = 5$ kcal/mol·Å^2) in a 0.5-ns constant-pressure (NPT) simulation, in order to allow the lipid molecules to pack against the protein surface, and for the area of the lipid bilayer to adjust accordingly. The NPT conditions were maintained after the 0.5-ns simulation and the protein was allowed to move freely, until the cross-sectional area stabilized (3.5 ns total unrestrained NPT simulations). Once the system area stabilized, further equilibration of 10 ns under constant area and normal pressure conditions (1 atm; NP_nAT ensemble) was performed.

The membrane-bound model was branched into four simulation systems after this initial equilibration: (A) MgATP-bound, full transporter; (B) nucleotide-free, full transporter; (C) after removing the periplasmic section (the entire MalE together with the MalF periplasmic loop MalF:E94–L258) from System B; and (D) after further removing the two MalK monomers from System C, i.e., only the TMDs without the periplasmic loop of MalF. The three truncated systems (B–D) were further equilibrated as follows. System B was equilibrated with the protein restrained for another 0.5 ns ($k = 5$ kcal/mol·Å^2), to adjust to the empty space introduced by the removal of the nucleotides. Since the construction of Systems C and D involved the removal of MalE (the BP) and a large deletion within the MalF polypeptide chain leaving a large space at the periplasmic side of the system, the protein and the surrounding lipid molecules in these two systems were re-solvated into smaller water boxes. Moreover, in order to avoid artificial effects at the truncation sites, the two introduced termini were capped with acetamide (N-terminus of MalF:T259) and N-methylamide (C-terminus of MalF:N93) groups, respectively. Systems C and D were further equilibrated with the protein restrained for 0.1 ns ($k = 5$ kcal/mol·Å^2), allowing proper solvation of the

exposed surfaces. All of the systems were then simulated further for 70 ns under equilibrium conditions, and each system (A–D) was simulated twice with different initial velocities randomly assigned to each atom. These systems are referred to as Systems A1, A2, B1, B2, C1, C2, D1, and D2. The four types of simulation systems are shown in the main article, Fig. 1, *A–D*.

Data Analysis

Data analysis and structure illustrations were done using VMD (13). The key conformational changes in the simulations were quantified as (i) the degree of dimer opening in the NBDs at the two nucleotide-binding sites, and (ii) the separation of the two coupling helices (EAA1), and that of the flanking helices (EAA2), which are positioned closer to the core of the TMDs (for graphical representations, refer to Fig. 1 *E* in the main article). The NBD dimer opening is measured by the center-of-mass distance between the RecA-like (MalK:P88–E151) and the helical (MalK:A2–Y87, P152–G235) subdomains of opposing monomers. Since the NBDs in the maltose transporter are homodimers, two values are reported for each time point, which are annotated as sites A and B, respectively. The separation of the two EAA1 helices is defined as the center-of-mass distance between the backbone atoms of MalF:P396–G407 and those of MalG:D185–G196, and the separation of the two EAA2 helices is defined using residues MalF:F411–L422 and MalG:W200–S211.

To characterize the structural elements responsible for the NBD-TMD coupling, generalized correlation between all C_α pairs was calculated using the toolkit g_correlation (14) in GROMACS 3 (15). In order to examine the relative movements of various structural elements at the NBD-TMD interface, the trajectories were superimposed onto the initial structure (equivalent to PDB:2R6G (1)) using the C_α atoms of the two EAA helices (either MalF:P396–L422 or MalG:D185–S211) and the C_α deviation of each residue in the flanking NBD was recorded for each frame (MalK monomer B for MalF superposition, and MalK monomer A for MalG superposition). The NBD C_α displacements and fluctuations calculated after these superpositions were then presented using their maximum and minimum values, the 25 and 75 percentiles, and the mean value. Similar structural alignments were employed to analyze and compare several crystal structures of other small ABC importers, in order to characterize the structural relationship between their NBDs and TMDs. These structures include: (I) the maltose transporter MalFGK in the inward-facing, nucleotide-

free state (PDB:3FH6 (16)), (II) the molybdate/tungstate transporter ModABC of *Archaeoglobus fulgidus* (PDB:2ONK (17)) for which the structural alignment was done using ModB:D155–S181, (III) the molybdate/tungstate transporter ModBC of *Methanosarcina acetivorans* (PDB:3D31 (18)) where structural alignment was done using ModB:D167–S193, and (IV) the methionine transporter MetNI of *Escherichia coli* (PDB:3DHW (19)) where structural alignment was done using MetN:P116–A142. As the NBDs in these transporters do not include the same number of C_α atoms, the C_α displacements and fluctuations were calculated only for the C_α atoms at equivalent positions derived from the structure-based sequence alignment shown in Fig. S1.

Similar analysis of the NBD-TMD coupling was also applied to other subfamilies of ABC transporters. For large ABC importers, the crystal structure of the *Escherichia coli* vitamin B_{12} transporter (BtuCDF, PDB:2QI9 (20)) was superimposed to a homologous structure (a putative metal-chelate importer HI1470/1, PDB:2NQ2 (21)), using the structural elements BtuC:S206–P227 and HI1471:S213–K234, while the C_α displacements and fluctuations of their NBDs were calculated based on the sequence alignment provided in the online supporting material of (21). For ABC exporters, the crystal structure of *Staphylococcus aureus* SAV1866 (PDB:2HYD (22)) was selected as the reference for superposition of structures of other ABC exporters, including several structures of bacterial lipid-A flippase MsbA (23) (from *Escherichia coli*, PDB:3B5W; from *Vibrio cholerae*, PDB:3B5X; and from *Salmonella typhimurium*, PDB:3B5Y,3B5Z,3B60), and the multidrug resistant protein Pgp of *Mus musculus* (PDB:3G5U (24)). The superposition at the NBD-TMD interface for ABC exporters was done using the combination of two NBD-contacting intracellular loops (ICLs): ICL1 from one TMD and ICL2 from the other TMD — in which ICL1 is defined as SAV1866:A106–Q116, MsbA:G/H110–S120, Pgp:N153–D163 (for NBD1 analysis), and Pgp:R794–K804 (for NBD2 analysis). ICL2 is defined as SAV1866:R206–I218, MsbA:M210–G222, Pgp:A896–R908 (for NBD1), and Pgp:V253–G265 (for NBD2). The analysis of NBD C_α atoms in ABC exporters was based on equivalent positions shown in the structure-based sequence alignment (Fig. S3).

Supplemental Figures

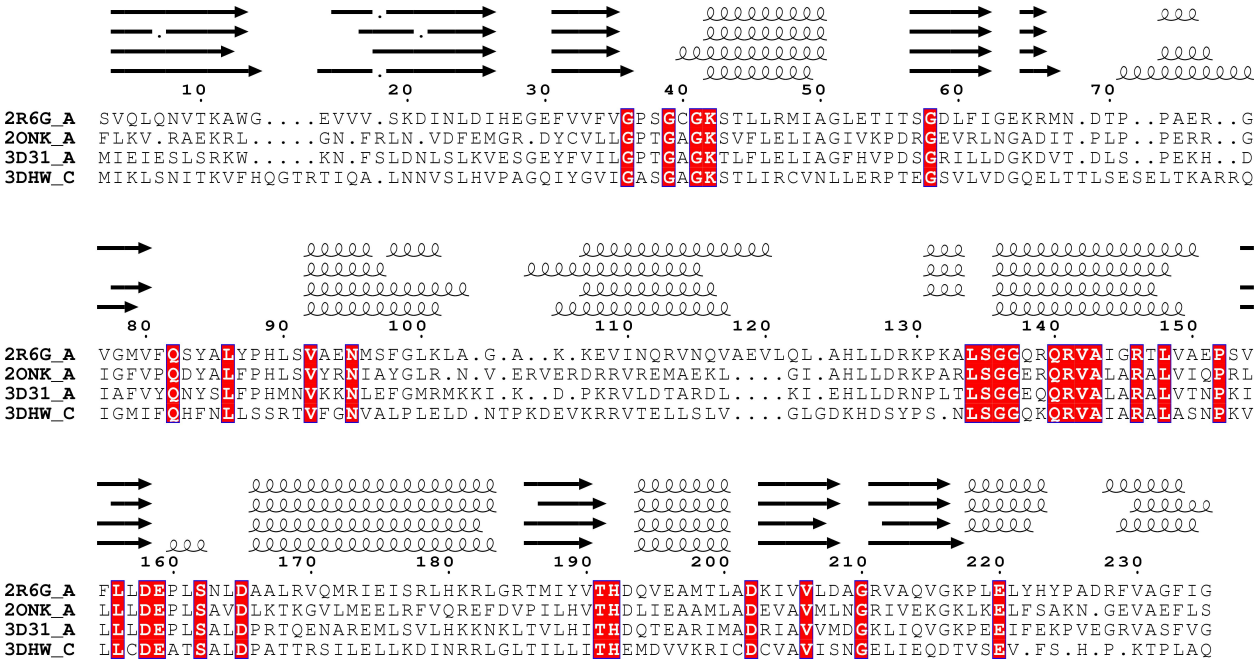

Figure S1:

Figure S1. Structure-based sequence alignment of NBDs in the small ABC importer fold. Four intact transporter complexes in the small ABC importer fold are structurally superimposed using their NBDs, corresponding to the region S3–G235 of MalK. The four crystal structures are: the maltose transporter MalEFGK of *Escherichia coli* (PDB: 2R6G), the molybdate/tungstate transporter ModABC of *Archaeoglobus fulgidus* (PDB: 2ONK), the molybdate/tungstate transporter ModBC of *Methanosarcina acetivorans* (PDB: 3D31), and the methionine transporter MetNI of *Escherichia coli* (PDB: 3DHW). Identical residues in the sequence alignment are boxed in red color. This sequence alignment is the basis of structural comparison of the NBD-TMD interface of this fold, as shown in Fig. 4 D of the main article.

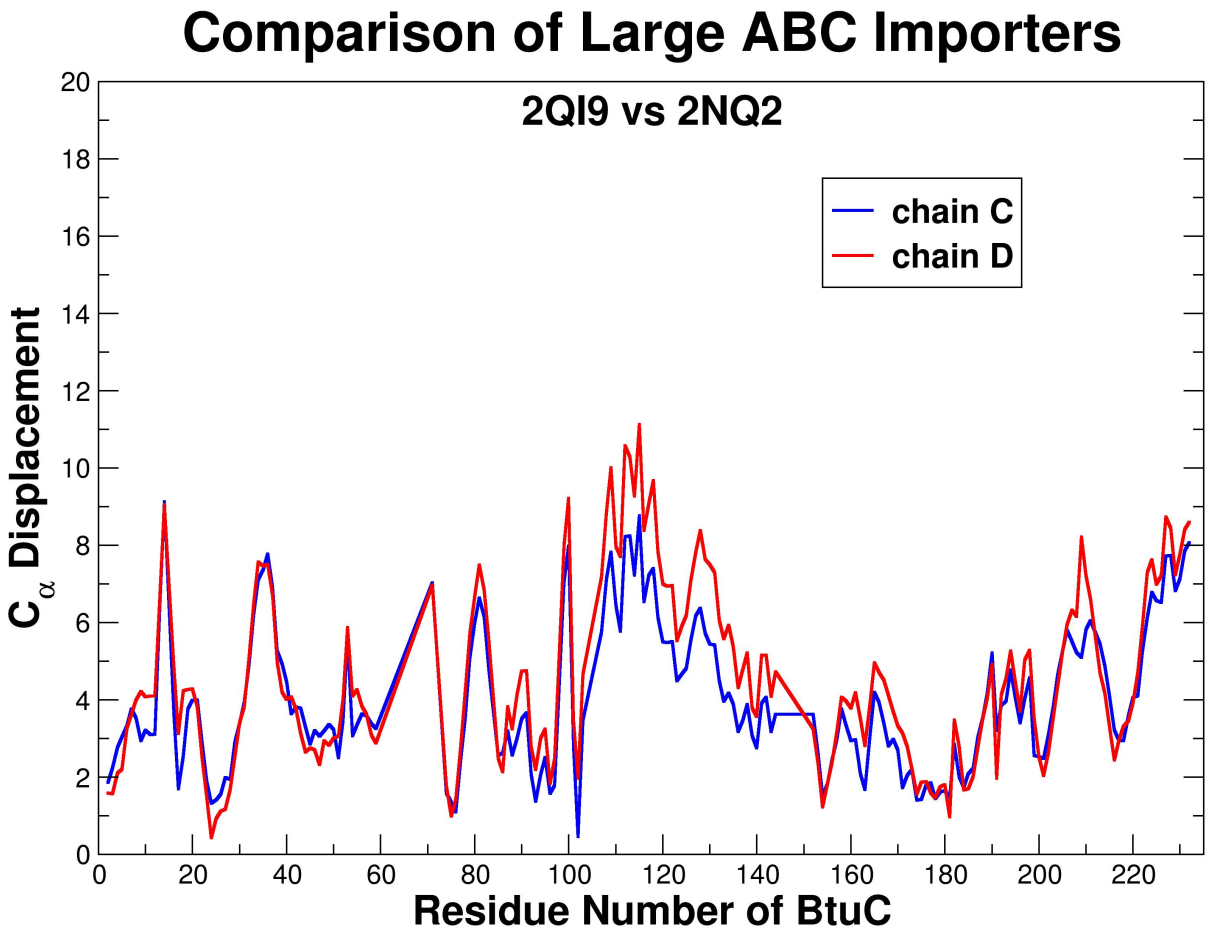

Figure S2:

Figure S2. The NBD-TMD coupling in BtuCDF and HI1470/1. The C_α displacement between BtuC and HI1470 when the crystal structures are superimposed at the EAA loops of BtuD and HI1471 (BtuD:S206–P227 in PDB: 2QI9, HI1471:S213–K234 in PDB: 2NQ2), similar to the methods of structural superposition and comparison described in the main article and illustrated in Fig. 3, C–F.

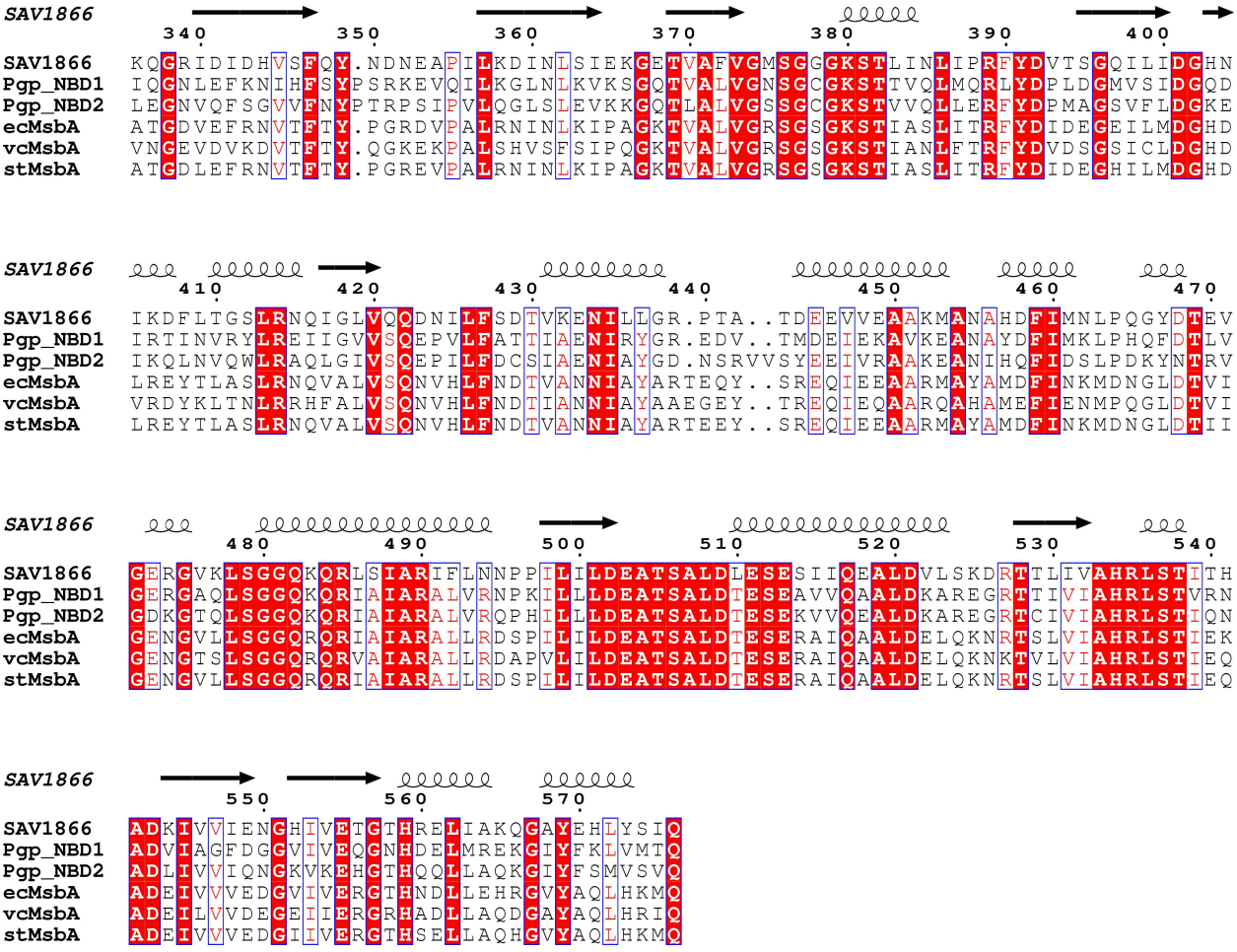

Figure S3:

Figure S3. Structure-based sequence alignment of NBDs in ABC exporters. Crystal structures of intact ABC exporters are superimposed to maximize the alignment of the region shown in the sequence. The alignment is produced in the same way as in Fig. S1. Crystal structures used are: 2HYD (SAV1866 of *Staphylococcus aureus*), 3G5U(P-glycoprotein of *Mus musculus*), 3B5W (MsbA of *Escherichia coli*), 3B5X (MsbA of *Vibrio cholerae*), 3B60 (MsbA of *Salmonella typhimurium*).

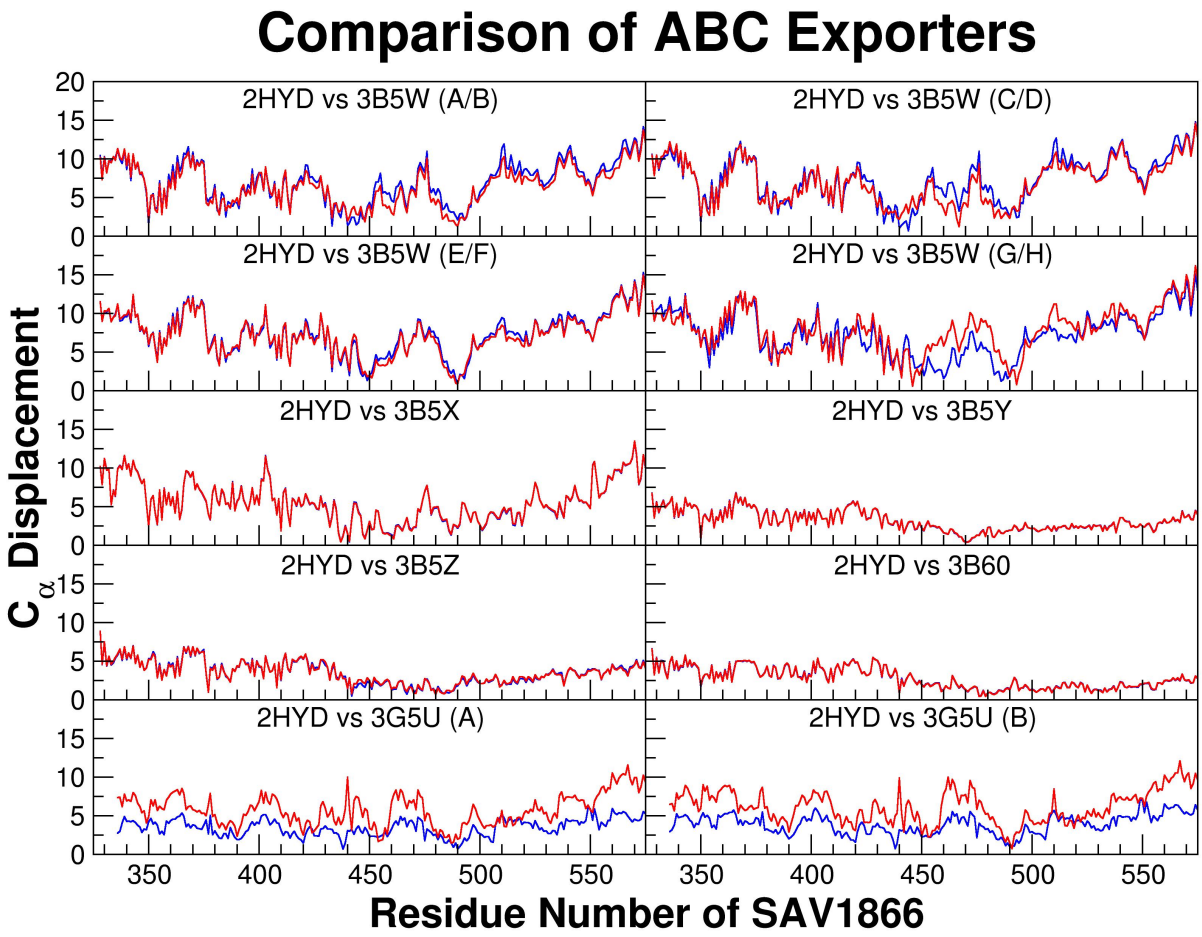

Figure S4:

Figure S4. The NBD-TMD coupling in ABC exporters. The C_α displacement between different ABC exporters listed in Fig. S3. The crystal structures are superimposed at the ICL1 of one TMD (SAV1866:A106–Q116, MsbA:G/H110–S120, Pgp:N153–D163 for NBD1 and Pgp:R794–K804 for NBD2) plus the ICL2 of the other TMD (SAV1866:R206–I218, MsbA:M210–G222, Pgp:A896–R908 for NBD1 and Pgp:V253–G265 for NBD2), and the C_α positions of the flanking NBD are compared. Since multiple crystal structures have been resolved for the *Salmonella typhimurium* MsbA, the PDB: 3B5Y, 3B5Z are also included in the comparison.

References

[1] Oldham, M. L., D. Khare, F. A. Quiocho, A. L. Davidson, and J. Chen. 2007. Crystal structure of a catalytic intermediate of the maltose transporter. *Nature.* 450:515–521.

[2] Chen, J., G. Lu, J. Lin, A. L. Davidson, and F. A. Quiocho. 2003. A tweezers-like motion of the ATP-binding cassette dimer in an ABC transport cycle. *Mol. Cell.* 12:651–661.

[3] Smith, P. C., N. Karpowich, L. Millen, J. E. Moody, J. Rosen, P. J. Thomas, and J. F. Hunt. 2002. ATP binding to the motor domain from an ABC transporter drives formation of a nucleotide sandwich dimer. *Mol. Cell.* 10:139–149.

[4] Phillips, J. C., R. Braun, W. Wang, J. Gumbart, E. Tajkhorshid, E. Villa, C. Chipot, R. D. Skeel, L. Kale, and K. Schulten. 2005. Scalable molecular dynamics with NAMD. *J. Comp. Chem.* 26:1781–1802.

[5] MacKerell Jr., A. D., M. Feig, and C. L. Brooks III. 2004. Extending the treatment of backbone energetics in protein force fields: Limitations of gas-phase quantum mechanics in reproducing protein conformational distributions in molecular dynamics simulations. *J. Comp. Chem.* 25:1400–1415.

[6] Feller, S. and J. A. D. MacKerell. 2000. An improved empirical potential energy function for molecular simulations of phospholipids. *J. Phys. Chem.* 104:7510–7515.

[7] Foloppe, N. and A. D. MacKerrell Jr. 2000. All-atom empirical force field for nucleic acids: I. parameter optimization based on small molecule and condensed phase macromolecular target data. *J. Comp. Chem.* 21:86–104.

[8] Jorgensen, W. L., J. Chandrasekhar, J. D. Madura, R. W. Impey, and M. L. Klein. 1983. Comparison of simple potential functions for simulating liquid water. *J. Chem. Phys.* 79:926–935.

[9] Kuttel, M., J. W. Brandy, and K. J. Naidoo. 2002. Carbohydrate solution simulations: Producing a force field with experimentally consistent primary alcohol rotational frequencies and populations. *J. Comp. Chem.* 23:1236–1243.

[10] Martyna, G. J., D. J. Tobias, and M. L. Klein. 1994. Constant pressure molecular dynamics algorithms. *J. Chem. Phys.* 101:4177–4189.

[11] Feller, S. E., Y. H. Zhang, R. W. Pastor, and B. R. Brooks. 1995. Constant pressure molecular dynamics simulation — the Langevin piston method. *J. Chem. Phys.* 103:4613–4621.

[12] Darden, T., D. York, and L. Pedersen. 1993. Particle mesh Ewald. An N·log(N) method for Ewald sums in large systems. *J. Chem. Phys.* 98:10089–10092.

[13] Humphrey, W., A. Dalke, and K. Schulten. 1996. VMD – Visual Molecular Dynamics. *J. Mol. Graphics.* 14:33–38.

[14] Lange, O. F. and H. Grubmüller. 2006. Generalized correlation for biomolecular dynamics. *Proteins: Struct., Func., Bioinf.* 62:1053–1061.

[15] Lindahl, E., B. Hess, and D. van der Spoel. 2001. GROMACS 3.0: A package for molecular simulation and trajectory analysis. *J. Mol. Mod.*

[16] Khare, D., M. L. Oldham, C. Orelle, A. L. Davidson, and J. Chen. 2009. Alternating access in maltose transporter mediated by rigid-body rotations. *Mol. Cell.* 33:528–536.

[17] Hollenstein, K., D. C. Frei, and K. P. Locher. 2007. Structure of an ABC transporter in complex with its binding protein. *Nature.* 446:213–216.

[18] Gerber, S., M. Comellas-Bigler, B. A. Goetz, and K. P. Locher. 2008. Structural basis of trans-inhibition in a molybdate/tungstate ABC transporter. *Science.* 321:246–250.

[19] Kadaba, N. S., J. T. Kaiser, E. Johnson, A. Lee, and D. C. Rees. 2008. The high-affinity *E. coli* methionine ABC transporter: Structure and allosteric regulation. *Science.* 321:250–253.

[20] Hvorup, R. N., B. A. Goetz, M. Niederer, K. Hollenstein, E. Perozo, and K. P. Locher. 2007. Asymmetry in the structure of the ABC transporter-binding protein complex BtuCD-BtuF. *Science.* 317:1387–1390.

[21] Pinkett, H. W., A. T. Lee, P. Lum, K. P. Locher, and D. C. Rees. 2007. An inward-facing conformation of a putative metal-chelate-type ABC transporter. *Science.* 315:373–377.

[22] Dawson, R. J. and K. P. Locher. 2006. Structure of a bacterial multidrug ABC transporter. *Nature.* 443:180–185.

[23] Ward, A., C. L. Reyes, J. Yu, C. B. Roth, and G. Chang. 2007. Flexibility in the ABC transporter MsbA: Alternating access with a twist. *Proc. Natl. Acad. Sci. USA*. 104:19005–19010.

[24] Aller, S. G., J. Yu, A. Ward, Y. Weng, S. Chittaboina, R. Zhuo, P. M. Harrell, Y. T. Trinh, Q. Zhang, I. L. Urbatsch, and G. Chang. 2009. Structure of P-glycoprotein reveals a molecular basis for poly-specific drug binding. *Science*. 323:1718–1722.